Nonlocal Interactions Stabilize Compact Folding Intermediates in Reduced Unfolded Bovine Pancreatic Trypsin Inhibitor†

David S. Gottfried‡ and Elisha Haas*

Department of Life Sciences, Bar-Ilan University, Ramat-Gan 52900, Israel

Received June 10, 1992; Revised Manuscript Received September 18, 1992

ABSTRACT: To further our understanding of the protein folding process, it is desirable to examine the structural intermediates (equilibrium and kinetic) that are populated between the statistical coil state and the folded molecule. X-ray crystallography and NMR structural studies are unable to determine long-range distances in proteins under denaturing solution conditions. Nonradiative (Förster) energy transfer, however, has been shown to be a spectroscopic ruler for the measurement of distance distributions and diffusion between selected sites in proteins under a range of different solution conditions. The distributions of distances between a donor probe at the N-terminal residue and an acceptor attached to one of the four lysine residues (15, 26, 41, 46) of reduced and unfolded (in 6 M guanidine hydrochloride and 20 mM dithiothreitol) bovine pancreatic trypsin inhibitor (BPTI) were measured as a function of temperature. Even in strong denaturant and reducing agent, BPTI does not exist as a statistical coil polypeptide. It appears that nonlocal (long-range) interactions are already beginning to "fold" the protein toward a more compact, native conformation. As the temperature is increased under these conditions, hydrophobic interactions lead to an even more compact structure consistent with the predictions of phase diagrams for globular proteins.

The folding pathway of a globular protein is a transition from an unfolded state, via folding intermediates, to the native folded state. Both the initial state and the intermediate states of the folding pathway are nonnative conformations of the protein (Anfinsen, 1961; Nemethy & Scheraga, 1979; Kim & Baldwin, 1982, 1990; Ptitsyn, 1987). The folding transition is a process in which chain segment–segment and chain–solvent interactions outweigh the large amount of chain entropy. The earliest intermediates in protein folding are naturally those which reduce the chain entropy significantly more than those intermediates formed in the later phases of the folding transition.

The early intermediates on the folding pathway are structures with local pockets of flexibility which may form from a statistical coil state. Such structures are by nature only partially stabilized; they undergo large fluctuations and should, therefore, be viewed as distributions of many microstates that change with the solution conditions (solvent, temperature, pH, etc.) or with the aminoacyl sequence. Such initial folding intermediates are defined and stabilized by local (short-range) and nonlocal (long-range) interactions (NLIs)[1] within and between chain segments, respectively (Chan & Dill, 1991; Oas & Kim, 1987). Both types of interactions in an unfolded state can be detected as deviations of a characteristic of the protein chain from that of a statistical coil (Chan & Dill, 1991; Dill & Shortle, 1991). Therefore, an investigation of the early folding intermediates of globular proteins, in a search for the specific interactions that generate the initial structures, depends on the measurement of intramolecular characteristics such as the end-to-end distance (EED) distributions of segments of the chain. It is the nonlocal interactions which are most effective in reducing chain entropy and, consequently, are most important in the initial stages of the folding pathway.

Some of the main difficulties in an experimental determination of intramolecular distributions include the "localization" of the measured signals to specific positions on the protein chain, the limited resolution, the low and transient population of the intermediate states, and the very limited solubility of the unfolded or partially folded conformers of globular proteins [see the reviews of Kim and Baldwin (1990), Dill and Shortle (1991), Montelione and Scheraga (1989), and Creighton (1978)]. We have recently developed a method for determination of segmental EED distributions and rates of conformational fluctuations in globular proteins which is based on time-resolved, dynamic, nonradiative energy transfer (ET) measurements (Haas, 1986; Amir & Haas, 1987; Beechem & Haas, 1989). We have shown that this approach can overcome some of the difficulties mentioned above and is very successful in the determination of the initial conformations of unfolded proteins at very low concentrations.

We have previously reported (Amir & Haas, 1987) the preparation of a series of fluorescent probe-labeled bovine pancreatic trypsin inhibitor (BPTI) derivatives, (1–*n*)BPTI (*n* = 15, 26, 41, 46), in which a (2-methoxy-1-naphthyl)-methylenyl group (MNA) is attached to the α-amino group of arginine, at position 1, and a [7-(dimethylamino)coumarin-4-yl]acetyl group (DA-coum) is attached via an amide bond to the ϵ-amino group of one of the four lysine residues (at position 15, 26, 41, or 46). This work is based on methods developed earlier (Haas et al., 1975; Haas, 1986) for nonradiative excitation energy transfer measurements and

† This work was supported by the Basic Research Fund of the Israeli Academy of Sciences, the Russle Foundation of Miami, and the NIH National Institute of General Medical Sciences (GM-39372). D.S.G. thanks the European Molecular Biology Organization for a postdoctoral fellowship.

* Address correspondence to this author.

‡ Current address: Department of Physiology and Biophysics, Albert Einstein College of Medicine, Bronx, NY 10461.

[1] Abbreviations: CFIS, chain folding initiation site; BPTI, bovine pancreatic trypsin inhibitor; (1–*n*)BPTI, N^{α}MNA-arg[1]-N^{ϵ}-DA-coum-lys^{n}-BPTI; DA-coum, [7-(dimethylamino)coumarin-4-yl]acetyl; (DA-coum)$_2$-BPTI, BPTI labeled by two DA-coum groups; DTT, dithiothreitol; EDTA, ethylenediaminetetraacetic acid; *E*, energy transfer efficiency (percent); EED, end-to-end distance; ET, energy transfer; GuHCl, guanidine hydrochloride; MNA, (2-methoxy-1-naphthyl)methylenyl; (MNA)$_2$-BPTI, BPTI labeled by two MNA groups; NLI, nonlocal interaction.

0006-2960/92/0431-12353$03.00/0

their analysis (Förster, 1948; Stryer & Haugland, 1967; Stryer, 1978). A new laser-based, time-resolved fluorometer with enhanced sensitivity and spectral and time resolution was used for fluorescence decay measurements, and a global analytical method was employed for fitting a model, which includes EED distributions and diffusion, to the data (Beechem & Haas, 1989). This has allowed the determination of segmental EED distributions in the unfolded protein and their dependence on the solvent and temperature. The measured EED distributions reveal compact structures in the BPTI chain even under reducing and unfolding conditions. The effect of temperature on the equilibrium structures (both compact and extended) indicates a cold unfolding transition in reduced BPTI. In addition, inferences can be made regarding the type of nonlocal interactions which are effective in stabilization of the compact conformations even in the presence of strong denaturant. The experiments reported here set the basis for a more detailed search for the specific residues responsible for these effective interactions and, consequently, the early intermediates in the folding pathway of BPTI.

MATERIALS AND METHODS

Sample Preparation. Preparation, purification, and characterization of the singly- and doubly-labeled protein derivatives were reported previously (Amir & Haas, 1987). The donor probe, (2-methoxy-1-naphthyl)methylenyl (MNA), was attached to the N-terminal arginine, while the acceptor, [7-(dimethylamino)coumarin-4-yl]acetyl (DA-coum), was attached to one of four lysine residues at positions 15, 26, 41, or 46. The structures of the probe chromophores and a schematic drawing of the protein showing the labeling sites are shown in Figure 1. The purity of the labeled protein derivatives was confirmed by absorption and fluorescence spectroscopy before all measurements, and the protein concentration was determined from the extinction of the acceptor band at 380 nm (Amir & Haas, 1986a). All reagents used in this study were as described previously (Amir & Haas, 1987).

Protein samples were reduced and denatured in a buffer solution containing 50 mM bicine (pH 8.5), 6 M guanidine hydrochloride (GuHCl), 1 mM EDTA, and 20 mM dithiothreitol (DTT) for at least 4 h at room temperature. Samples were allowed to refold (in the reduced state) by dilution 12-fold into a final DTT concentration of 4 mM and GuHCl concentration of 0.5 M (Amir & Haas, 1988).

Fluorescence Lifetime Measurements. The time-correlated single photon counting system used for our measurements is based substantially on one previously described (Beechem et al., 1990). The light source for the fluorescence decay apparatus is a mode-locked, frequency-doubled Nd:YAG laser (Coherent Antares 76-YAG) which synchronously pumps a dye laser (Coherent 701-2CD) using Kiton Red as the active medium. The cavity-dumped dye laser output produces pulses in the wavelength range 600–670 nm with pulse widths of 5 ps (measured using an in-house designed and built autocorrelator) and repetition rates up to 3.8 MHz. The output from the dye laser is frequency doubled from the visible to the near ultraviolet wavelengths. The pulse train is focused onto a BBO type I crystal (CSK Co., Inc.) to generate pulses in the wavelength range 300–335 nm with energies up to 0.25 nJ/pulse (0.5–1.0 mW at 3.8 MHz). The polarization of the resulting light is rotated to the desired angle for excitation using a double Fresnel rhomb (Optics for Research).

In a unique design, the sample cuvette (a custom-made cylindrical quartz cell of 5-mm outer diameter and 3-mm

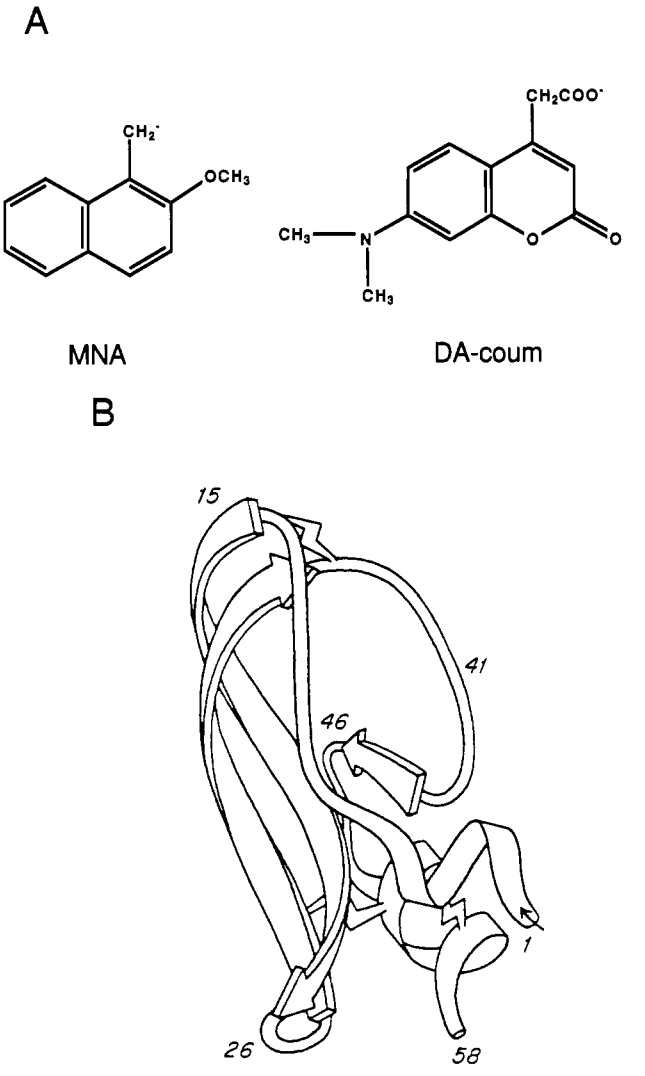

FIGURE 1: (A) Structures of donor, (2-methoxy-1-naphthyl)-methylenyl (MNA), and acceptor, [7-(dimethylamino)coumarin-4-yl]acetyl (DA-coum), chromophores. (B) Ribbon drawing of bovine pancreatic trypsin inhibitor showing labeling positions used in this study.

inner diameter requiring less than 50 μL of solution) is illuminated from below by the laser beam. The cuvette is held in a copper cell holder which is temperature-stabilized using a thermostatically controlled water/ethylene glycol bath. The fluorescence, collected at right angles to the illuminating light from the side of the sample cell, is collimated and passed through a Glan–Thomson polarizer and then a filter (optional). The emission is focused onto the entrance slit of a $^1/_4$ m monochromator (Jobin-Yvon HR-250) with a 300 groove/mm grating (12 nm/mm dispersion) whose output is focused onto the cathode of a fast photomultiplier tube (PMT, Phillips XP2020Q) biased at 2700 V. The rotation of the emission polarizer, selection of the emission filters, and wavelength of the monochromator are all controlled externally by computer.

The output of the detector is input to a constant-fraction discriminator (CFD, Tennelec 453) which provides the start input for a time-to-amplitude converter (TAC, Tennelec 862). The stop pulse for the TAC is provided by the cavity dumper sync output. The TAC output is read by a combination analog-to-digital converter and multichannel analyzer (ADC/MCA, Nucleus PCA-II with 1024 channels) in a PC-AT (80286 based) computer with an Intel 80287 math coprocessor. This combination of start and stop pulses for the TAC results in fluorescence decays in reverse time, but this is corrected

numerically prior to analysis. Using a typical 2-MHz repetition rate of the laser, pulse detection rates up to 50 kHz are possible without pulse pileup errors; however, the emission pulse rates were usually reduced to 20 kHz (1% of illumination rate) by attenuation of the laser intensity. Using the detection arrangement and electronics as described, the instrument response function is typically 800 ps FWHM.

Although a considerable amount of previous work has been published in which a scattering compound (e.g., a suspension of polystyrene beads in methanol) has been used to reproduce the instrument response function, we have chosen to use a reference compound of short, monoexponential fluorescence decay time. The use of reference and mimic compounds has been found to significantly reduce experimental artifacts due to color shift, monochromator path length dispersion, and photocathode targeting response (Zuker et al., 1985; James et al., 1983). We have found that the most stable and useful compounds for our wavelength regions of interest are PBD/ethanol (τ = 1.10 ns, 320–400 nm) and POPOP/ethanol (τ = 1.37 ns, 400–500 nm). The solutions are prepared fresh for each experiment and are tested for monoexponential decay using freshly prepared solutions of samples with known monoexponential emission decay (binaphthyl or anthracene). Data were also collected on solutions containing all components except the labeled protein for use in background subtraction.

Energy Transfer Data Analysis. Donor fluorescence decays in the absence and presence of the acceptor probe were obtained with excitation at 323 nm and emission collected at 360 nm. Acceptor fluorescence decays in the presence of the donor were obtained with 323-nm excitation and 475-nm emission. Acceptor-only decays were collected either through use of an acceptor-only labeled protein (excitation at 323 nm; emission at 475 nm) or excitation of the doubly-labeled protein at 380 nm and collection of the emission using a long-pass filter with $\lambda > 450$ nm (using a flash-lamp lifetime apparatus from Edinborough Instruments).

Determination of the energy transfer efficiencies was done using the donor-only lifetime and the average lifetime of the donor in the doubly-labeled protein calculated from a least-squares multiexponential fitting procedure. The average lifetime is given by

$$\langle\tau\rangle = \sum_{i=1}^{n}\alpha_i\tau_i / \sum_{i=1}^{n}\alpha_i \qquad (1)$$

where n is generally 3 and α_i and τ_i are the amplitude and lifetime, respectively, of the ith component. The energy transfer efficiency (E) is then given by $E = 1 - (\tau_{da}/\tau_d)$, where the "da" and "d" subscripts refer to donor–acceptor and donor-only labeled samples, respectively.

Deconvolution and global analysis of the donor-only, acceptor-only, and doubly-labeled probe emission decay curves was achieved using a Marquardt, nonlinear least squares method. The improvement in confidence interval for the parameters extracted from the analysis has been previously demonstrated (Beechem & Haas, 1989; Amir & Haas, 1987). In short, the decay curves were fit to the solution of the second-order partial differential equation which takes into account both the energy transfer perturbation term and diffusion between multiple conformations (Haas et al., 1978a; Beecham & Haas, 1989):

$$\frac{\partial\bar{N}(r,t)}{\partial t} = -\frac{1}{\tau_D}\left[1 + \frac{R_0^6}{r^6}\right]\bar{N}(r,t) + \frac{1}{N_0(r)}\frac{\partial}{\partial r}\left[N_0(r)D(r)\frac{\partial\bar{N}(r,t)}{\partial r}\right] \qquad (2)$$

The experimental decay curve is given by

$$I_D(t) = k\int_{r_{min}}^{r_{max}} N_0(r)\bar{N}(r,t)\,dr \qquad (3)$$

where $N_0(r) = N^*(r,0)$, $\bar{N}(r,t) = N^*(r,t)/N_0(r)$, $D(r)$ is the relative diffusion coefficient of the segments carrying the two probes, and τ_D is the lifetime of the excited state of the donor in the absence of an acceptor. Solution of eq 2 is obtained by numerical methods subject to the absorbing boundary conditions: $\bar{N}(r,0) = 1$ (normalization), $N(0,t) = 0$, and $N(r_{max},t) = 0$. $N_0(r)$ is the equilibrium distance distribution, and $N^*(r,t)$ is the time-dependent, normalized (at $t = 0$) distribution of interprobe distances for molecules with an excited donor probe. The equilibrium distance is modeled using a skewed Gaussian profile (Edwards, 1965). $N^*(r,t)$ contains contributions from spontaneous fluorescence decay, energy transfer, and three-dimensional Fick-type diffusion of the probes relative to each other (Beechem & Haas, 1989). Although the equation given above is for a single equilibrium distance distribution, the treatment can be generalized for multiple-component distributions. For most of the data presented here, two-component distributions are required in the model to sufficiently fit the data. Implications of this finding are discussed below.

In the static case, where the Brownian motions of the segments are slow on the time scale of the measurements, the EED distribution can be obtained using the integral directly:

$$I_D(t) = k\int_{r_{min}}^{r_{max}} N_0(r)\exp[-t/\tau_d[1 + (R_0/r)^6]]\,dr \qquad (4)$$

where k is a proportionality factor and r_{min} and r_{max} are the end-to-end distances (EED) of closest approach and of a fully extended conformation, respectively. In eq 4, R_0 and τ are known from independent experiments, $I_D(t)$ is measured experimentally, and thus $N_0(r)$ can be reconstructed by curve fitting methods.

The quantum yields, overlap integrals, and R_0 parameters found in the Förster energy transfer equation were determined as previously described (Amir & Haas, 1987; Beals et al., 1991). The orientation factor (κ^2) was estimated as $^2/_3$ (Haas, 1978a).

RESULTS

Average Energy Transfer Efficiency. The average energy transfer efficiencies (E) for the four doubly-labeled samples in reducing/unfolding conditions (20 mM DTT, 6 M GuHCl) at temperatures of 1, 20, and 35 °C along with those for the native protein at 20 °C are given in Table I and shown graphically in Figure 2. The transfer efficiency data for the 1–26 labeled protein in reduced/refolding conditions (4 mM DTT, 0.5 M GuHCl) are also given in Table I. An example of the donor lifetime measurement in the absence and presence of the acceptor [for (1–26)BPTI in 0.5 M GuHCl] is shown in Figure 3. The donor-only decay (Figure 3a) was fit with a single-exponential lifetime of 6.4 ns ($\chi^2 = 1.2$). The donor decay with acceptor present (Figure 3b) is shown fit to a single exponential which results in an unsatisfactory fit ($\chi^2 = 64$). A fit to a three-exponential decay is also shown and

Table I: Energy Transfer Efficiencies in Donor–Acceptor Labeled BPTI

solution[a]	temp (°C)	τ_d (ns)[b]	E(%)[c] 1–15[d]	1–26	1–41	1–46
6 M GuHCl	1	4.54 ± 0.04	39.0 ± 2.0	13.6 ± 0.7	3.7 ± 0.2	11.2 ± 0.6
6 M GuHCl	20	4.38 ± 0.04	53.3 ± 2.7	34.8 ± 1.7	27.8 ± 1.4	27.8 ± 1.4
6 M GuHCl	35	4.08 ± 0.03	57.7 ± 2.9	52.2 ± 2.6	43.4 ± 2.2	33.5 ± 1.7
0.5 M GuHCl	1	6.79 ± 0.07		52.1 ± 2.6		
0.5 M GuHCl	20	6.36 ± 0.07		62.4 ± 3.1		
0.5 M GuHCl	35	5.94 ± 0.08		80.3 ± 4.0		
0 M GuHCl[e]	20	6.8	44 ± 5	84 ± 5	85 ± 5	80 ± 5

[a] Other solution conditions: 50 mM bicine (pH 8.5), 1 mM EDTA, and 4–20 mM DTT (except in native). [b] Donor lifetime in donor-only labeled protein. Errors correspond to 98% confidence interval. [c] Transfer efficiency calculated from a multiexponential analysis of the donor fluorescence. Errors estimated from rigorous error analysis are ±5% of the reported value. [d] Numbers represent labeling positions of donor–acceptor probes. [e] Data for native state are from Amir and Haas (1987).

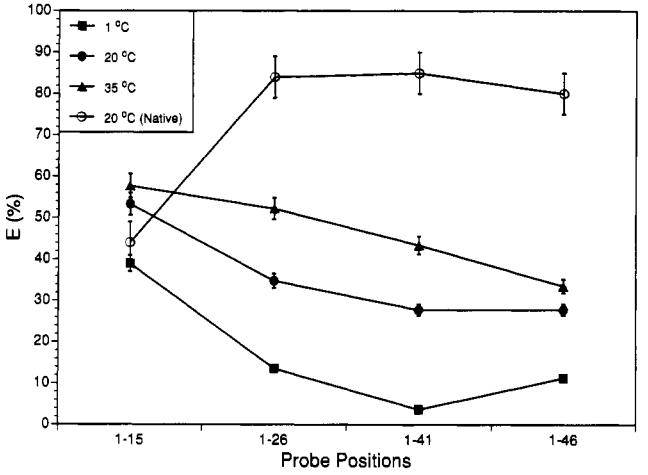

FIGURE 2: Average energy transfer efficiencies between donor and acceptor on BPTI in 6 M GuHCl calculated using multiexponential fits to the donor fluorescence decay. Average lifetimes were calculated according to $\langle\tau\rangle = \sum\alpha_i\tau_i/\sum\alpha_i$, where $i = 1 - 3$ and α_i and τ_i are the amplitude and lifetime, respectively, of the ith component. The energy transfer efficiency, E, is then given by $E = 1 - (\tau_{da}/\tau_d)$, where the "d" and "da" subscripts refer to donor-only and donor–acceptor labeled samples, respectively. Error bars reflect the 98% confidence interval. Data for the native state (O) are taken from Amir and Haas (1987).

results in an average lifetime of 2.4 ns ($\chi^2 = 1.6$). The quality of the fits were determined from the value of χ^2, the residuals, and the autocorrelation of the residuals (Grinvald & Steinberg, 1974).

As was reported previously (Amir & Haas, 1988), the reduced unfolded state of BPTI in 6 M GuHCl shows a significant decrease in the energy transfer efficiency for the four doubly-labeled protein derivatives, compared to the native state, with the exception of (1–15)BPTI. Only at low temperature (see Figure 2) does the transfer efficiency of (1–15)BPTI decrease below that of the native state. Under certain conditions, as was observed previously (Amir & Haas, 1987), the reduced unfolded state of BPTI in 6 M GuHCl shows a nonmonotonic decrease of E with segment length. At low temperature, the transfer efficiency observed for the derivative (1–46)BPTI, in which 46 amino acid residues separate the two labeled residues, is comparable to that obtained for (1–26)BPTI, a derivative in which the labeled segment is only 26 residues long.

Simple polymer theory (Flory, 1953; Chan & Dill, 1991) and empirical studies (Tanford, 1968) indicate that the average distance between chain ends for proteins in the statistical coil configuration should follow a monotonically increasing dependence on the number of amino acid residues. The excluded volume effect in unordered protein chains increases this dependence. Most theoretical estimations and experimental measurements [e.g., Tanford (1968)] of segmental EED distributions of unfolded proteins have been made for long segments. The results shown in Figure 2 and Table I are for relatively short polypeptide segments. In addition, the transfer efficiencies can also be increased by segmental diffusion which enhances the transfer rate (Haas, 1986). However, even at this level of approximation, Figure 2 indicates that in 6 M GuHCl at neutral pH, BPTI is not in a statistical coil conformation. This is confirmed by the detailed distance distribution analysis reported below.

The temperature dependence of E reveals two phenomena: (1) At high temperature (35 °C), the dependence of the energy transfer efficiency on the number of amino acid residues between the probes is consistent with the expected behavior. That is, a decrease in transfer efficiency with increased segment length is observed. At low temperature (1 °C), however, there is an increase in E from the 41 residue to the 46 residue separation. In the simplest interpretation (assuming a static, narrow distance distribution), this corresponds to a decrease in the average interprobe distance. As will be discussed further in the following section, this behavior, under the conditions of this experiment, is inconsistent with a simple understanding of the conformation of unfolded proteins and may be an indication of nonlocal interactions which stabilize intersegmental structures. (2) For all four segment lengths measured, E increases with temperature. This can result from an increase in chain dynamics or a decrease in the segmental EED. These two contributions are resolved by the detailed analyses of the time-resolved experiments presented in the following sections.

Finally, Table I also contains data for (1–26)BPTI under refolding conditions (0.5 M GuHCl). The energy transfer efficiencies are intermediate between those found in 6 M GuHCl at all temperatures and those measured under native conditions.

Determination of Distance Distributions. The measurements of energy transfer efficiencies alone cannot be used for detailed structural characterization because the rate of energy transfer, a measure proportional to the transfer efficiency, from a donor chromophore to an acceptor chromophore on a protein molecule is determined by both the equilibrium EED distribution and the interprobe diffusion constant. Using global analysis (Beechem & Haas, 1989; Beals et al., 1991), we have attempted to determine the two contributions individually. In the course of the data analysis, it was found that, for the present pair of probes under the conditions of the experiments, the correlation between the parameters of the equilibrium EED distribution and the intramolecular diffusion parameter limited the statistical significance of the extracted diffusion parameter. However, as has been shown by simulations and by rigorous analyses of fluorescence decay

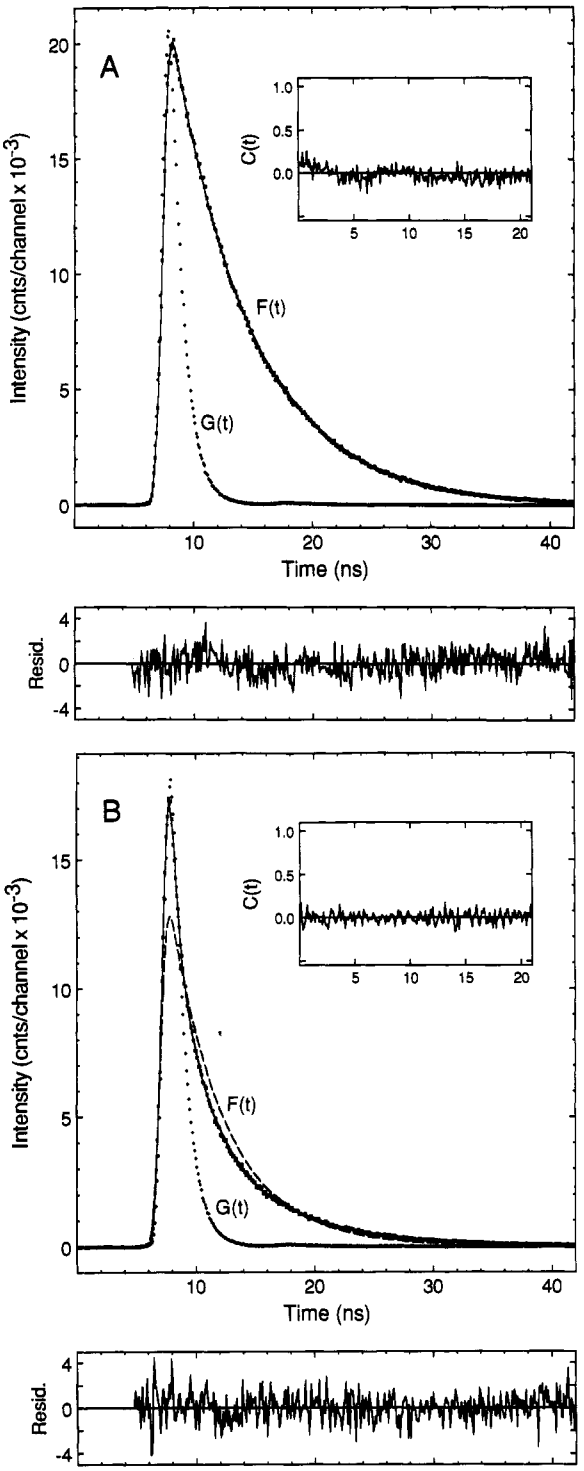

FIGURE 3: Example of multiexponential fit of donor fluorescence decay in the presence of acceptor chromophore showing the decrease in donor lifetime due to resonant energy transfer. (A) Decay of the donor-only labeled protein, (1-MNA)BPTI, and a fit to a single exponential (τ = 6.4 ns, χ^2 = 1.2). (B) Decay of the donor-acceptor labeled protein, (1–26)BPTI, and a fit to three exponentials ($\langle\tau\rangle$ = 2.4 ns, χ^2 = 1.6). A fit to one exponential (χ^2 = 64) is shown as a dashed line for comparison. Solution conditions were 50 mM bicine, pH 8.5, 0.5 M GuHCl, 1 mM EDTA, and 4 mM DTT, at 20 °C. Samples were excited at 323 nm, and the decay was monitored at 360 nm (6-nm bandwidth). The decay of the reference compound (PBD/ethanol) used for deconvolution of the excitation profile is shown as $G(t)$. The fluorescence [$F(t)$] is shown with the fits. The residuals and autocorrelation of the residuals, $C(t)$, are also shown.

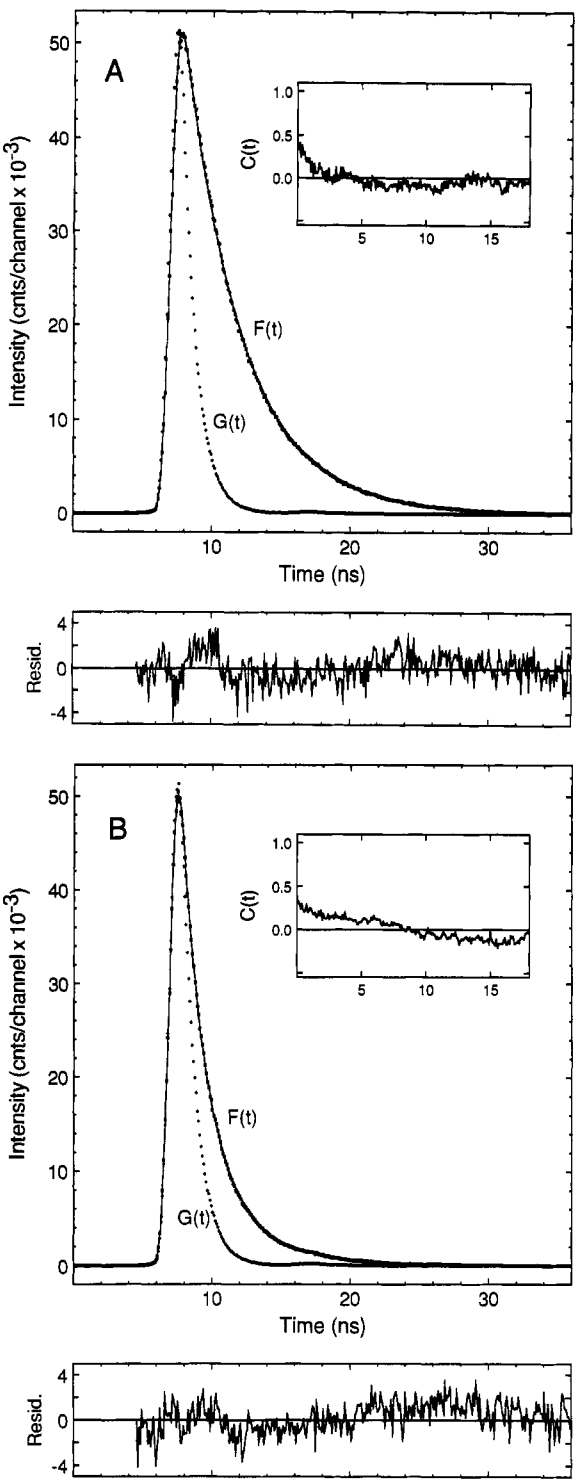

FIGURE 4: Example of global fitting of fluorescence decay to a model including energy transfer and intersegmental diffusion. (A) Decay of the donor-only labeled protein, (1-MNA)BPTI, and a fit to a single exponential (τ = 4.1 ns, local χ^2 = 1.9). (B) Decay of the donor-acceptor labeled protein, (1–15)BPTI in 6 M GuHCl and 20 mM DTT at 35 °C, and the fit from a global analysis of four decay curves (see the text for details). The local χ^2 = 2.1 and the global fit has χ^2 = 2.3. The fitting parameters are given in Table II. All other sample and experimental conditions are as described in the legend to Figure 3.

curves, the statistical significance of the values determined for the parameters of the EED distributions, the mean and the width parameters, is satisfactory.

The fitting of a donor decay (in the presence of acceptor) to a model which includes energy transfer and intramolecular diffusion is shown in Figure 4. In most cases, the fluorescence decay data could not be satisfactorily fit using global analysis (based on values of χ^2 and autocorrelation of the residuals) to a simple model (comprising a single distance distribution

Table II: End-to-End Distance Distributions for Protein Segments in Reduced and Denatured BPTI

sample[a]	temp (°C)	R, W (Å)[b]	χ^2 [c]	R_1, W_1 (Å)[d]	R_2, W_2 (Å)[e]	f[f]	D (Å/ns)[g]	χ^2 [c]
1–15	1	28.0	5.6	24.2–24.9	65.5	0.55–0.65	4–17	3.6
		8.0		1.3–4.9	20.0			
	20	26.0	5.0	24.4–29.4	65.5	0.65–0.80	0–6	2.6
		6.0		2.3–6.2	20.0			
	35	24.5	2.8	23.3–25.4	65.5	0.66–0.91	0–25	2.3
		5.0		4.2–7.4	20.0			
1–26	20	34.8	16.9	23.1–26.4	45.0	0.35–0.45	0–2	4.4
		7.3		1.8–4.7	10.0			
	35	29.5	6.1	24.5–26.0	45.0	0.55–0.62	0–5	2.4
		7.8		2.6–5.2	10.0			
1–41	20	39.8	7.5	21.0–23.4	50.0	0.2–0.4	0–4	6.0
		13.4		2.0–6.0	10.0			
	35	40.0	4.4	25.7–26.7	55.0	0.44–0.51	0–16	3.0
		8.7		2.2–5.5	11.0			
1–46	20	39.5–43.6	7.4	*h*			0–8	
		12.3–20.0						
	35	33.3	15.0	18.8–30.5	45.0	0.25–0.85	0–16	4.7
		10.9		4.1–10.4	10.0			

[a] Numbers represent donor–acceptor labeling positions. [b] Peak (R, upper) and standard deviation (W, lower) of the distance distribution for a fit to one distribution. [c] χ^2 value for a global fit of the experimental data set (four decay curves). [d] Peak (R_1, upper) and standard deviation (W_1, lower) of the variable distance distribution for a fit to two distributions. The range given is from a rigorous error analysis (Beechem & Haas, 1989) and represents the 98% confidence interval. [e] Peak (R_2, upper) and standard deviation (W_2, lower) of the fixed distance distribution for a two distributions fit. The choice of parameters is made empirically from a rigorous error analysis. [f] Fractional population represented by distribution 1 in a bimodal fit. [g] Confidence interval for the diffusion constant. An upper bound of 25 Å/ns was applied. [h] Single broad distribution gave the same quality of fit as the bimodal distribution in this experiment.

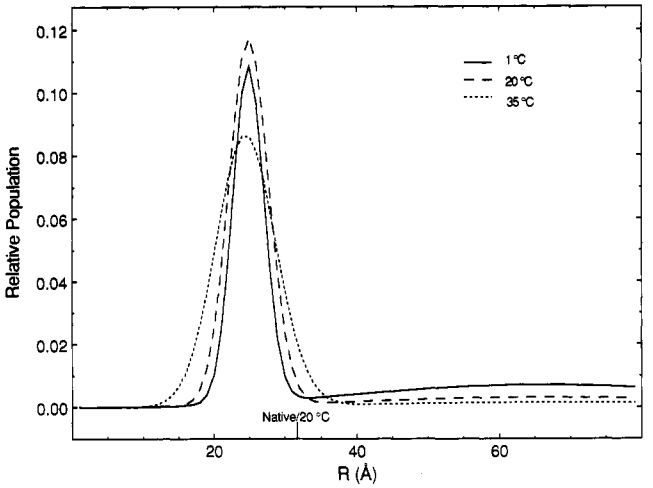

FIGURE 5: Temperature dependence of the end-to-end distance (EED) distribution functions for (1–15)BPTI in 6 M GuHCl and 20 mM DTT calculated from a global analysis for the donor and acceptor decay curves. The distance for the 1–15 segment in the native state (31.7 Å) calculated from the X-ray crystal coordinates (Wlodawer et al., 1984) is shown along the x-axis for comparison.

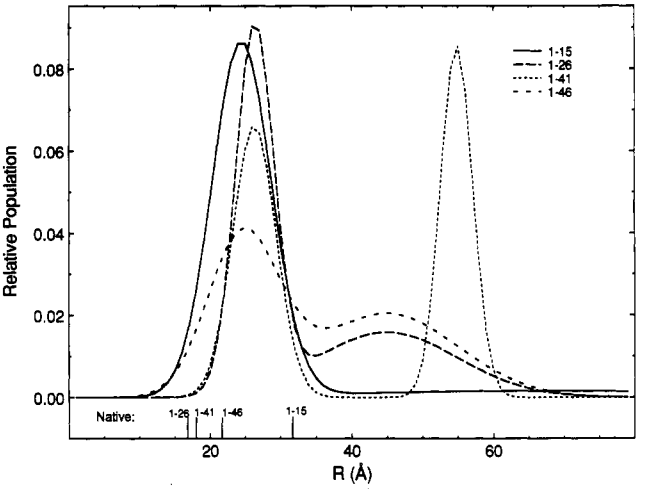

FIGURE 6: EED distribution functions for the four protein segments in 6 M GuHCl and 20 mM DTT at 35 °C calculated from a global analysis of the donor and acceptor decay curves. The distances for the same segments calculated from the X-ray crystal coordinates are shown along the x-axis for comparison.

and diffusion constant) which has been used successfully for the same BPTI derivatives in the native state (Amir & Haas, 1987). This clearly shows that at least two distinct subpopulations, a compact one with an average EED in the range of 20–30 Å and a second expanded subpopulation with a large interprobe distance, were required for the analyses. We chose the procedure of adding a second distance distribution with fixed peak distance and width parameters, which were determined empirically by a grid search. The characteristics of the segmental EED distributions and the diffusion parameters obtained by global analysis of the donor and the acceptor fluorescence decay curves of the four double-labeled derivatives in 6 M GuHCl are listed in Table II. The effect of temperature on the EED distance distribution for the (1–15)BPTI derivative is shown in Figure 5. As was expected from the energy transfer efficiency measurements, the average distance found at all three temperatures, approximately 24.5 ± 2.0 Å, is significantly shorter than the distance measured in the native state (Amir & Haas, 1987), in the unfolded state in a glycerol/GuHCl solvent mixture (Amir et al., 1992), or in the native state calculated from the crystal structure coordinates (Wlodawer et al., 1984). The short, narrow distribution component is accompanied by a fraction of molecules with large interprobe distances. The rather large width of this second distribution and the large distance between the probes (relative to R_0 = 26.0 Å) precludes a more precise determination of the shape of the EED distribution of this subpopulation and physical interpretation of its conformation (see below). As the temperature is increased from 1 to 35 °C, the relative proportion of the subpopulation with the large EED decreases. The equilibrium shifts in favor of the compact structure, accompanied by an increase in the width of this distribution component. Figure 6 illustrates the distance distributions of all four double-labeled BPTI derivatives used in the present study at a temperature of 35 °C.

Although the two subpopulation model improved the goodness of fit in most cases (as judged by a significant decrease

in the global χ^2), the data for some samples at certain temperatures could not be fit even with this expanded model. In those cases which could be fit, the second distribution which was required for the best fit was found to include very long interprobe distances corresponding to an expanded conformation of the protein backbone. In the Förster model of energy transfer, however, any separation between the donor and acceptor of greater than approximately $2.0R_0$ has negligible energy transfer efficiency and consequently will possess a large uncertainty interval. Therefore, we make no attempt to ascribe much physical significance to the exact shape of this distribution. The interpretation of the experiments is simply that, in the reduced/unfolded state, PBTI exists as an equilibrium mixture of at least two conformational subpopulations, and one subpopulation was usually found to be in a compact conformation. As will be discussed in greater detail below, this has important implications for a structural analysis of the unfolded state and of the refolding intermediate states.

The results shown in Table II and Figures 5 and 6 provide information on the conformational characteristics of BPTI in the reduced unfolded state. Even in 6 M GuHCl, reduced BPTI is not in a statistical coil conformation, and the different segment lengths and temperatures studied reveal local features which are of interest for understanding the mechanism of folding of BPTI. The distance distributions for the 1–26 and 1–41 derivatives, which probe the distance between the N terminus and the central segment of the chain which forms the hydrophobic core, are split between two subpopulations even at elevated temperatures. The distribution of the distances between residues 1 and 46 is characteristic of the distance between the chain termini, and the compact subpopulation in this end-to-end distance of the entire molecule clearly deviates from that expected for a statistical coil state of unfolded BPTI. This is evidence for specific long-range interactions between the polypeptide chain termini, resulting in an attraction between the terminal segments even under unfolding conditions. It is important to note that a nonspecific compaction (e.g., by hydrophobic collapse alone) would have yielded a considerably larger average EED in the compact component of (1–46)BPTI, as compared to that of (1–26)-BPTI. We propose that this interaction is a significant contribution to reduction of the chain entropy and that it may be a signal for a chain folding initiation site (CFIS). The segment 1–15 is closer to a single distribution with an average distance that may be shorter than that expected for a statistical coil (see Discussion). The temperature dependence of the distance between residues 1 and 15 (Figure 5) shows decreased population of the extended conformation and increased width of the compact conformer with increasing temperature. It appears that this short segment is folded due to an interaction with the remainder of the protein at higher temperatures.[2]

These results indicate that, even under the drastic perturbation of the reducing and denaturing solvent conditions, nonlocal (long-range) interactions (NLIs) can stabilize compact conformers in BPTI. The compact conformations could be a result of nonspecific general hydrophobic condensation (solvent exclusion), or they may be specific folding intermediates with native-like local subdomain structures. In either case, very stable NLIs are effective in the formation of compact structures. The current set of labeled derivatives detect NLIs within the N-terminal segment [(1–15)BPTI and (1–26)-BPTI] and between the N-terminal and the C-terminal segments [(1–46)BPTI]. These interacting regions can be thought of as chain folding initiation sites similar to those proposed by Nemethy and Scheraga (1979).

DISCUSSION

The experiments reported here were designed for the detection and characterization of the initial folding intermediates of BPTI, a small globular protein. The goal of these experiments was to search for the presence of structure in BPTI under conditions in which it has previously been considered to be fully unfolded (Creighton, 1978). The time-resolved, nonradiative energy transfer measurements in the donor–acceptor labeled BPTI derivatives reveal a compact structure, very different from a statistical coil, even in the reduced, unfolded (denatured) state. A detailed analysis of intra- and intersegmental EEDs indicates that nonlocal interactions in the protein are effective even under these conditions. Local and nonlocal interactions responsible for compact structure in unfolded BPTI are assumed to be essential elements in the initiation and direction of its folding pathway. This discussion will first examine some experimental constraints and the range of statistical confidence intervals for the results, and then possible interpretations will be presented.

This work is part of a continuing study of BPTI folding intermediates (Amir et al., 1992). The same donor–acceptor labeled derivatives have been previously studied using steady-state methods and lower resolution time-resolved measurements in viscous solvents. The more precise experimental and analytical methods described in this report have enabled these most recent experiments to reveal additional details. In general, the conclusions of the earlier work (Amir & Haas, 1987, 1988) are supported by the present results. The main advantage of the present set of experiments and the introduction of global analysis of the data is that glycerol is not required in the solvent to reduce conformational fluctuations. Furthermore, the new apparatus introduced here has greatly improved the spectral and time resolution of the measurements. The main difference between the earlier and the present results is that, in the absence of glycerol, we find a further reduction of the transfer efficiencies at low temperature in the derivatives (1–26)BPTI, (1–41)BPTI, and (1–46)BPTI. For (1–15)-BPTI in the reduced unfolded state, we find a shorter average of the EED distribution and, at low temperature, a second extended subpopulation. This second subpopulation disappears at higher temperatures and could not be detected in the previous experiments. The effect of glycerol on protein conformation, as discussed elsewhere (Amir et al., 1992), may well be the source of these differences.

Control Experiments. Interpretation of the results presented here is based on rigorous chemical and spectral characterizations of the labeled derivatives published earlier (Amir & Haas, 1986a,b; Amir et al., 1986, 1992; Haas, 1986). Conclusions are based on global analyses of the fluorescence decay kinetics of both the donor and the acceptor which have been discussed in detail previously (Haas et al., 1978a; Beechem & Haas, 1989). The essential control experiments and possible errors (e.g., the orientation problem) have already been discussed in detail with regard to the set of derivatives used here (Amir & Haas, 1987, 1988; Amir et al., 1992) and will only be summarized below.

All of the fluorescent probe-labeled protein derivatives were active and regained quantitative inhibitory activity after

[2] A possible cause for this effect may be hydrophobic interaction with the core of the molecule. This compaction is also seen in the temperature dependence of the EED distribution measured for (1–26)BPTI in the reduced state in 0.5 M GuHCl. It is found that the increase of E with temperature (see Table I) is caused primarily by a decreased EED rather than enhanced chain fluctuations (D. S. Gottfried and E. Haas, unpublished results).

unfolding and refolding. Decreases in energy transfer efficiencies were probably not caused by loss of labels under the unfolding conditions, as the refolded derivatives regained the fluorescence transfer efficiencies observed for the native state prior to unfolding. The absence of intermolecular energy transfer under the experimental conditions (defined by the concentration, temperature, and solvent composition) was confirmed by measurement of the donor fluorescence decay and excitation spectrum in a 2:1 mixture of $(MNA)_2$-BPTI and $(DA\text{-}coum)_2$-BPTI (3–10 μM). No intermolecular energy transfer was detected under these conditions, which implies that aggregation does not occur to a significant degree, while the average distance between protein molecules in solution in the absence of aggregation allows only a negligible energy transfer rate.

No dependence of the results on DTT concentration was found, and no oxidized disulfides were found in doubly-labeled BPTI under reducing conditions (Amir & Haas, 1988; Creighton, 1977). Furthermore, the concentration of DTT did not decrease below 2 mM before or during the measurements. A possible influence of the probes on the chain conformation has been discussed (Amir et al., 1992); in the absence of glycerol such effects should be further reduced.

Spectroscopic Considerations. Our analysis of time-resolved energy transfer measurements depends strongly on two parameters: τ_D, the donor fluorescence decay constant in the absence of an acceptor, and R_0, the Förster constant. τ_D was measured for each experiment using MNA-BPTI, a protein derivative labeled only with the donor attached at the same site as in the doubly-labeled derivatives. Monoexponential decays were obtained for MNA-BPTI under all the experimental conditions employed in the present study. Thus, all specific effects induced by the changing conditions (e.g., temperature, solvent components, and instrumental parameters) were automatically taken into account. By inclusion of this reference experiment in the global analysis without prior processing, no assumptions, corrections, or approximations are made. R_0 was calculated using the experimentally determined refractive index, donor fluorescence quantum yield, and acceptor absorption and donor emission spectra under each set of conditions. Thus, changes in transfer efficiency due to molecular and spectroscopic effects of solvent and temperature were also taken into account by their effect on R_0.

A frequently cited potential source of uncertainty in the magnitude of R_0 is the dependence of transfer probabilities on the relative orientations of the two probes. Two uncertainties are involved: (1) the possible contribution of distributions of orientations to the observed distribution of transfer efficiencies and (2) the most probable average R_0 for each derivative. This issue has been discussed in detail by many authors (Jones, 1970; Hillel & Wu, 1976; Stryer, 1978; Dale et al., 1979). On the basis of the above sources, we have already presented a complete discussion of theoretical and experimental considerations leading to the conclusion that the probability for a value of R_0 differing by more than 10% from the dynamically averaged R_0 ($\kappa^2 = {}^2/_3$) is small (Haas et al., 1978b). In other work (Amir et al., 1992), we have shown that, even in viscous solutions, dynamic averaging of the probe orientations is effective. The higher temperatures and lower viscosities of the solutions used in all of the experiments reported here further reduce any uncertainties due to orientation effects.

Data Analysis. Global analysis is a data fitting procedure which reduces uncertainty that arises due to correlations between fitting parameters (Beechem & Haas, 1989). This allows a determination of the equilibrium segmental EED distributions, $N_0(r)$ in eq 3, in flexible chains free of bias due to the enhancement of energy transfer by diffusion (Haas et al., 1978a). However, in most of the experiments reported here, the fit of the experimental decay curves achieved with simple models of EED distribution and diffusion are unsatisfactory as determined by the fitting statistics (reduced χ^2, residuals, and autocorrelation of the residuals). Parameters which are outside the bounds of the physical system are also found. Assuming that the experimental data is not artifactual, this implies that the model used is not a perfect representation of the real system. Adjustments to the model function could include a complex composition of conformational subpopulations in the unfolded chains, asymmetric shapes of the EED distributions, and distance-dependent diffusion coefficients (it is conceivable that the conformers with extreme EED are less flexible than the conformers with an average EED); however, with the present pair of chromophores, the additional parameters needed to expand the model in these ways would increase the uncertainty in all determined parameters. It is our experience that the parameters characterizing the EED distribution, the mean of the distribution and, to a lesser extent, the width, are very well recovered, independent of the features of the model functions used for the analysis, and that these are good first approximations of the correct distribution. This is demonstrated by the relatively narrow uncertainty invervals for these parameters determined from a rigorous error analysis (see Table II). The fine details of the shape of the edges of the model EED distributions do not affect the quality of the fit since these fractions contribute either very long or very short decay components which have weak distance dependences. Simulation studies show that a pair of probes with lower direct excitation of the acceptor and a larger ratio of τ_D/τ_A can allow the addition of parameters to the analysis without loss of statistical significance.

At low temperature, the distributions measured for reduced BPTI in 6 M GuHCl consisted of at least two subpopulations. A fit to a single-component distribution gives a skewed distribution with increased population at the edges of the EED distribution and poor fitting statistics (see Table II). The improvement in fit gained by the two-population model is significant as judged by the reduced χ^2 and distributions of the residuals. However, not all data sets resulted in adequate fits using even this expanded model. Consequently, there are probably other features, including those listed above, which are not represented by the present simple model. Furthermore, for the probes used in the present experiments (R_0 = 26.0 Å), the donor lifetime is only weakly distance-dependent at distances larger than 50 Å. Therefore the shapes of the distributions corresponding to the fully unfolded state should be considered as approximations only.

The Reduced Unfolded State. The specific aim of the present study was to search for nonlocal (long-range) interactions in the reduced unfolded state of BPTI. It is our hypothesis that these interactions play a major role in the determination of the initial intermediate states in the folding pathways of globular proteins. The evidence presented here leads to the fundamental conclusion that, even under drastic unfolding conditions of 6 M GuHCl and 20 mM DTT at 35 °C, BPTI is not in a statistical coil conformation. The series of four labeled derivatives used span a wide range of end-to-end segment length, from 15 to 46 residues. A polypeptide chain in a statistical coil state is expected to show both a single-component EED distribution and a monotonically

increasing average EED as a function of the number of monomer units in the segment (Flory, 1953). If nonlocal interactions are small, the mean squared EED is given by $\langle R_n^2 \rangle = Cnl^2$ where $C = 1$, n is the number of monomers, and l is the bond length (Yamakawa, 1971; Chan & Dill, 1991). This succinctly states that, when local interactions dominate, the mean square EED is proportional to the chain length. If energy transfer efficiency is an approximate measure of probe separation, then Figure 2 clearly shows that random coil statistics are not valid for reduced BPTI in 6 M GuHCl. It is of interest to compare the average distances obtained for the labeled BPTI derivatives with those expected for a polypeptide of comparable length in a random coil conformation. However, we are not aware of experimental determinations of EED distributions for polypeptides in the statistical coil state in the solvents used in this study. Although Flory and co-workers (Brant & Flory, 1965a,b; Brant et al., 1967) have calculated the expected average EED for long polypeptide chains in ideal solvents, these conditions are not met by the present measurements. Earlier time-resolved ET measurements of a series of model peptides known to be in the statistical coil state showed single-component EED distributions (Haas et al., 1975). A decapeptide (the longest peptide measured in that study) has an average EED of 22 Å. A conservative extrapolation of the results obtained by Haas et al. (1975) shows that average EEDs in the range 21–30 Å, observed for the compact sub-populations of the labeled BPTI derivatives (segmental lengths of 26–46 residues, see Table II), are inconsistent with the statistical coil state. Measurements of the EED distributions of a new series of doubly-labeled flexible oligopeptides of up to 26 residues are currently in progress.

The present results also differ from the chain length dependence of proteins unfolded in GuHCl determined by Tanford for large protein molecules (Tanford, 1968). In particular, at low temperature the average transfer efficiency for segments of length 26 and 46 residues are not very different. Table II shows that the EED distributions of the segments 1–15, 1–26, 1–41, and 1–46 have a major subpopulation with an average distance close to 25 Å. At low temperature this effect is more pronounced, perhaps due to reduced exchange and stabilization of nonlocal interactions. The results imply that nonlocal interactions (Chan & Dill, 1991) sufficiently strong to maintain considerable probability of intersegmental contacts are effective in BPTI even under conditions which have previously been considered unfolding. A comparison of the EED distributions of segments 1–26 and 1–46 implies a specific interaction between the N-terminal and the C-terminal segments of the protein backbone. We propose that this nonlocal interaction is a very effective force in directing the formation of early folding intermediates. A single nonlocal interaction can contribute a maximal reduction of chain entropy when it occurs between the two ends of the linear chain which is being folded. The existence of this interaction is probably an important element in the code for the initial steps of the folding pathway. The next problem is, of course, to identify the residues that contribute this interaction. In the native state, this conformation is secured by the 5–55 disulfide bond. Here we see that there are additional residues that stabilize an interaction between the two terminal segments prior to the formation of the disulfide bond.

Figures 2 and 5 show a striking temperature-dependent transition of the reduced, unfolded protein. As the temperature is increased from 1 to 35 °C, the transfer efficiencies for all the segments increase, and, for (1–15)BPTI, the extended conformers disappear while the compact conformers show a broader distribution of the EED. The increased transfer efficiency may be a result of contributions from an enhanced rate of conformational fluctuations or decreased EEDs. Figure 5 clearly shows that the second effect is dominant, at least for the 1–15 segment. At higher temperatures the subpopulation with the long EED distribution is decreased and the compact subpopulation is increased without a significant shift of its average EED. Thus, despite the large uncertainty in our current determination of the diffusion coefficient, it is clear that increased chain dynamics are not the dominant factor in the transfer efficiency enhancement, since it would have either appeared as a high value of the diffusion coefficient or as a shift of the EED distribution toward shorter distances.

These observations are likely due to a combination of factors. Nonlocal hydrophobic interactions are enhanced by high temperature and stabilize the compact conformers (which increases the transfer rate) without a large increase in conformational fluctuations. The reduced effectiveness of these interactions at low temperature result in an increase in population of the extended conformers and what appears like "cold unfolding" (Tanford, 1968; Privalov & Gill, 1988). Other, more specific nonlocal interactions, possibly hydrogen bonds or Van der Waals interactions, are more effective at low temperature and contribute to the nonstatistical chain length dependence of the EED.

In the reduced unfolded state, the N-terminal segment (residues 1–15) has an EED distribution with an average shorter than that of the native state at temperatures of 20 and 35 °C. This has also been observed in glycerol/GuHCl mixtures (Amir et al., 1992). A subpopulation with an extended conformation is found at low temperature. One possible interpretation of this result is that at low temperature some specific nonlocal interactions maintain a population of extended conformation (perhaps by an interaction between the two loops, residues 12–17 and residues 35–40) which is locked in the native state by the 14–38 disulfide bond. At room temperature and above, this segment is relaxed to a more compact conformation.

The temperature dependence of the overall protein compactness is in agreement with the phase diagrams which have been previously proposed for small globular proteins (Tanford, 1968; Ptitsyn, 1987; Shakhnovich & Finkelstein, 1989). These phase diagrams predict the possibility of cold denaturation and a heat-induced increase in protein compactness (i.e., the formation of a compact globule state). However, there is some disagreement in the literature as to the nature of the transitions between the phases. The present work is consistent with previous suggestions of a first-order transition between the unfolded and intermediate states (Shakhnovich & Finkelstein, 1989).

The results of the present time-resolved energy transfer measurements indicate several major characteristics of the initial phases of the folding pathway of BPTI. The chain is folded into a compact conformation even in a very unfavorable (in the context of folding) solvent and in the absence of the three disulfide bonds.[3] If we make the assumption that equilibrium conformations under unfavorable folding conditions are representative of the kinetic conformations most likely to form in the early stages of the folding pathway, then the observations discussed above support the hypothesis that the early folding intermediates of BPTI are in an equilibrium

[3] The distinction between denatured, meaning any nonnative conformation, and unfolded, referring to a statistical coil structure, has been pointed out by Dill and Shortle (1991), and we see evidence for this here.

between compact and extended (perhaps an unfolded, statistical coil) conformations. The formation of the compact globule is probably elicited by a combination of a hydrophobic condensation and a limited number of specifically coded, nonlocal, intersegment interactions. Both effects reduce the chain entropy and thus accelerate the folding transition. The initial condensation of the chain reduces the conformational space available by exclusion of the solvent and initiation of internal rearrangements which are transfer reactions between segments and, therefore, require exploration of a reduced section of the total conformational space. The crystal structure of native BPTI (Wlodawer et al., 1984) supports the hypothesis that four nonlocal (very long range) interactions may be sufficient to direct the pathway of folding of BPTI to the native conformation: an interaction between the two loops at the ends of the β structure (represented by the distance between residues 15 and 38), interactions between the N terminus and the β structure and the N terminus with the C terminus, and an interaction between the C-terminal segment and the β structure. These interactions alone can drastically reduce the conformational entropy of the unfolded chain and direct the pathway toward the native structure.

ACKNOWLEDGMENT

We thank Dr. E. Katchalski-Katzir for his interest and encouragement, Dr. I. Z. Steinberg for illuminating discussions, Dr. M. Rosenbluh for his advice and support in the design and operation of the laser system, Drs. G. L. Haberland, E. Wiskhofer, and A. G. Bayer for the generous gift of Trasylol, Drs. D. Amir and D. P. Levy for help in the preparation of the labeled BPTI derivatives, G. Haran for help with the analysis and discussions, and Dr. V. Itach for the rigorous analysis of many experiments. The excellent technical support by D. Friedman, E. Zimmerman, and N. Schwalb was essential for the construction and operation of the laser-based, time-resolved spectrofluorometer.

REFERENCES

Anfinsen, C. B., Haber, E., Sela, M., & White, F. H., Jr. (1961) *Proc. Natl. Acad. Sci. U.S.A. 47*, 1309–1314.
Amir, D., & Haas, E. (1986a) *Int. J. Pept. Protein Res. 27*, 7–17.
Amir, D., & Haas, E. (1986b) *Biopolymers 25*, 235–240.
Amir, D., & Haas, E. (1987) *Biochemistry 26*, 2161–2175.
Amir, D., & Haas, E. (1988) *Biochemistry 27*, 8889–8893.
Amir, D., Levy, D. P., Levin, Y., & Haas, E. (1986) *Biopolymers 25*, 1645–1658.
Amir, D., Krausz, S., & Haas, E. (1992) *Proteins: Struct. Funct. Genet. 13*, 162–173.
Beals, J. M., Haas, E., Krausz, S., & Scheraga, H. A. (1991) *Biochemistry 30*, 7680–7692.
Beechem, J. M., & Haas, E. (1989) *Biophys. J. 55*, 245–269.
Beechem, J. M., James, E., & Brand, L. (1990) in *Time-Resolved Laser Spectroscopy in Biochemistry II*, SPIE Proceedings, Vol. 1204, pp 686–698.
Brant, D. A., & Flory, P. J. (1965a) *J. Am. Chem. Soc. 87*, 2788–2791.
Brant, D. A., & Flory, P. J. (1965b) *J. Am. Chem. Soc. 87*, 2791–2800.
Brant, D. A., Miller, W. G., & Flory, P. J. (1967) *J. Mol. Biol. 23*, 47–65.
Chan, H. S., & Dill, K. A. (1991) *Annu. Rev. Biophys. Biophys. Chem. 20*, 447–490.
Creighton, T. E. (1977) *J. Mol. Biol. 113*, 313–328.
Creighton, T. E. (1978) *Prog. Biophys. Mol. Biol. 33*, 231–287.
Dale, R. E., Eisinger, J., & Blumberg, W. E. (1979) *Biophys. J. 26*, 161–194.
Dill, K. A., & Shortle, D. (1991) *Annu. Rev. Biochem. 60*, 795–825.
Edelhoch, H. A. (1967) *Biochemistry 6*, 1948–1954.
Edwards, S. F. (1965) *Proc. Phys. Soc. London 85*, 613–624.
Flory, P. J. (1953) *Principles of Polymer Chemistry*, Cornell University Press, Ithaca, NY.
Förster, T. H. (1948) *Ann. Phys. (Leipzig) 2*, 55–75.
Garel, J. R. (1978) *J. Mol. Biol. 118*, 331–345.
Grinvald, A., & Steinberg, I. Z. (1974) *Anal. Biochem. 59*, 583–598.
Haas, E. (1986) in *Photophysical and Photochemical Tools in Polymer Science* (Winnik, M. A., Ed.) pp 310–341, D. Reidel, Dordrecht.
Haas, E., Wilcheck, M., Steinberg, I. F., & Katchalski-Katzir, E. (1975) *Proc. Natl. Acad. Sci. U.S.A. 72*, 1807–1811.
Haas, E., Katchalski-Katzir, E., & Steinberg, I. Z. (1978a) *Biopolymers 17*, 11–31.
Haas, E., Katchalski-Katzir, E., & Steinberg, I. Z. (1978b) *Biochemistry 17*, 5064–5070.
Hillel, Z., & Wu, C. W. (1976) *Biochemistry 15*, 2105–2113.
James, D. R., Demmer, D. R. M., Verrall, R. E., & Steer, R. P. (1983) *Rev. Sci. Instrum. 54*, 1121–1130.
Jones, R. E. (1970) Ph.D. Thesis, Stanford University.
Kim, P. S., & Baldwin, R. L. (1982) *Annu. Rev. Biochem. 51*, 459–489.
Kim, P. S., & Baldwin, R. L. (1990) *Annu. Rev. Biochem. 59*, 631–660.
Montelione, G. T., & Scheraga, H. A. (1989) *Acc. Chem. Res. 22*, 70–76.
Nemethy, G., & Scheraga, H. A. (1979) *Proc. Natl. Acad. Sci. U.S.A. 76*, 6050–6054.
Oas, T. G., & Kim, P. S. (1988) *Nature 336*, 42–48.
Pace, C. N., & Tanford, C. (1968) *Biochemistry 7*, 198–208.
Privalov, P., & Gill, S. (1988) *Adv. Protein Chem. 39*, 191–234.
Ptitysin, O. B. (1987) *J. Protein Chem. 6*, 273–293.
Saxena, P., & Wetlaufer, D. B. (1970) *Biochemistry 9*, 5015–5022.
Shakhnovich, E. T., & Finkelstein, A. V. (1989) *Biopolymers 28*, 1681–1694.
Stryer, L. (1978) *Annu. Rev. Biochem. 47*, 819–846.
Stryer, L., & Haugland, R. P. (1967) *Proc. Natl. Acad. Sci. U.S.A. 58*, 719–226.
Tanford, C. (1968) *Adv. Protein Chem. 23*, 121–282.
Tanford, C. (1970) *Adv. Protein Chem. 24*, 1–95.
White, F. H., Jr. (1976) *Biochemistry 15*, 2906–2912.
Wlodawer, A., Walter, J., Huber, R., & Sjolin, L. (1984) *J. Mol. Biol. 180*, 301–329.
Yamakawa, H. (1971) *Modern Theory of Polymer Solutions*, Harper and Row, New York.
Zuker, M., Szabo, A. G., Bramall, L., & Krajcarski, D. T. (1985) *Rev. Sci. Instrum. 56*, 14–22.

Registry No. BPTI, 9087-70-1.